Acta Crystallographica Section D
Biological Crystallography
ISSN 0907-4449

Structures of *Staphylococcus aureus* peptide deformylase in complex with two classes of new inhibitors

Sang Jae Lee,[a,b] Seung-Jae Lee,[c] Seung Kyu Lee,[d] Hye-Jin Yoon,[b] Hyung Ho Lee,[e] Kyeong Kyu Kim,[f] Bong Jin Lee,[d,g]* Byung Il Lee[a]* and Se Won Suh[b,h]*

[a]Biomolecular Function Research Branch, Division of Convergence Technology, Research Institute, National Cancer Center, Goyang, Gyeonggi 410-749, Republic of Korea, [b]Department of Chemistry, College of Natural Sciences, Seoul National University, Seoul 151-742, Republic of Korea, [c]Howard Hughes Medical Institute and W. M. Keck Structural Biology Laboratory, Cold Spring Harbor Laboratory, 1 Bungtown Road, Cold Spring Harbor, NY 11724, USA, [d]Research Institute of Pharmaceutical Sciences, College of Pharmacy, Seoul National University, Seoul 151-742, Republic of Korea, [e]Department of Chemistry, Kookmin University, 861-1 Jeongneung, Seongbuk, Seoul 136-702, Republic of Korea, [f]Department of Molecular Cell Biology, Sungkyunkwan University of Medicine, Suwon, Gyeonggi 440-746, Republic of Korea, [g]ProMediTech Ltd, College of Pharmacy, Seoul National University, Seoul 151-742, Republic of Korea, and [h]Department of Biophysics and Chemical Biology, College of Natural Sciences, Seoul National University, Seoul 151-742, Republic of Korea

Correspondence e-mail: lbj@nmr.snu.ac.kr, bilee@ncc.re.kr, sewonsuh@snu.ac.kr

Received 25 November 2011
Accepted 19 March 2012

PDB References: peptide deformylase, complex with PMT387, 3u7k; complex with PMT497, 3u7l; complex with PMT1039, 3u7m; complex with PMT1067, 3u7n.

Peptide deformylase (PDF) catalyzes the removal of the formyl group from the N-terminal methionine residue in newly synthesized polypeptides, which is an essential process in bacteria. Four new inhibitors of PDF that belong to two different classes, hydroxamate/pseudopeptide compounds [PMT387 (7a) and PMT497] and reverse-hydroxamate/non-peptide compounds [PMT1039 (15e) and PMT1067], have been developed. These compounds inhibited the growth of several pathogens involved in respiratory-tract infections, such as *Streptococcus pneumoniae*, *Moraxella catarrhalis* and *Haemophilus influenzae*, and leading nosocomial pathogens such as *Staphylococcus aureus* and *Klebsiella pneumoniae* with a minimum inhibitory concentration (MIC) in the range 0.1–0.8 mg ml^{-1}. Interestingly, the reverse-hydroxamate/non-peptide compounds showed a 250-fold higher antimicrobial activity towards *S. aureus*, although the four compounds showed similar K_i values against *S. aureus* PDF enzymes, with K_i values in the 11–85 n*M* range. To provide a structural basis for the discovery of additional PDF inhibitors, the crystal structures of *S. aureus* PDF in complex with the four inhibitors were determined at resolutions of 1.90–2.30 Å. The inhibitor-bound structures displayed distinct deviations depending on the inhibitor class. The distance between the Zn^{2+} ion and the carbonyl O atom of the hydroxamate inhibitors (or the hydroxyl O atom of the reverse-hydroxamate inhibitors) appears to be correlated to *S. aureus* inhibition activity. The structural information reported in this study should aid in the discovery of new PDF inhibitors that can be used as novel antibacterial drugs.

1. Introduction

Bacterial infections are one of the leading causes of human death in the world (Boucher *et al.*, 2009; World Health Organization, 2004). Furthermore, the development of new antibacterial drugs is lagging behind the increasing rate of antibiotic resistance, which is becoming a major threat to human health (Boucher *et al.*, 2009; Spellberg *et al.*, 2004). Many currently used antibiotics will eventually become ineffective because of the acquisition of resistance mechanisms by pathogenic bacteria (Aubart & Zalacain, 2006; Boucher *et al.*, 2009). Therefore, there is an urgent need for the discovery of new antibacterial targets and the development of novel antibacterial agents. Peptide deformylase (PDF), a metalloenzyme that is highly conserved in bacteria, has been proposed as one attractive such target (Meinnel *et al.*, 1993; Solbiati *et al.*, 1999). It catalyzes the removal of a formyl group from the N-terminal methionine residue of newly synthesized polypeptides. Removal of the N-formyl group from nascent

polypeptide chains is an essential process in bacteria (Guillon *et al.*, 1992; Mazel *et al.*, 1994).

Bacterial PDFs are classified into two types. Type I PDFs are found in Gram-negative and Gram-positive bacteria, while type II PDFs are only found in Gram-positive bacteria (Guilloteau *et al.*, 2002). The sequence identity between type I and type II PDFs is relatively low (27–40%). Although the sequence identity ranges from 52 to 61% among PDFs of the same type, the C-terminal regions are markedly different despite similarity in the structures of type I and type II PDFs. In type I PDFs the C-terminal region consists of α-helices, whereas in type II PDFs the C-terminal region is comprised of β-strands that fold back onto themselves to form β-sheets. In addition, type I and type II PDFs share structurally conserved active sites that contain a metal ion. Crystal structures of inhibitor-bound PDFs are available for type I and type II enzymes. Type I PDFs from *Escherichia coli* (Clements *et al.*, 2001; Guilloteau *et al.*, 2002; Smith *et al.*, 2003), *Pseudomonas aeruginosa* (Guilloteau *et al.*, 2002; Molteni *et al.*, 2004; Yoon *et al.*, 2004), *Bacillus cereus* (Moon *et al.*, 2005), *Helicobacter pylori* (Cai *et al.*, 2006) and *Mycobacterium tuberculosis* (Pichota *et al.*, 2008) have been structurally characterized. The crystal structures of type II PDFs from *B. stearothermophilus* (Guilloteau *et al.*, 2002), *Streptococcus pneumoniae* (Smith *et al.*, 2003) and *S. aureus* (Yoon *et al.*, 2004) have also been reported. The structure of the *Leptospira interrogans* PDF, which is not classified as either type I or type II, has also been determined (Zhou *et al.*, 2004). *Plasmodium falciparum* is a unicellular eukaryotic protozoan that is a major human pathogen and the causative agent of the most deadly form of malaria; a crystal structure of its type I PDF has been reported (Robien *et al.*, 2004).

Actinonin, a naturally occurring hydroxamate pseudopeptide (Chen *et al.*, 2000), is a potent inhibitor of bacterial PDFs and has served as a template for drug discovery against bacterial PDFs. Two PDF inhibitors have advanced to phase I clinical studies: BB-83698 (Oscient Pharmaceuticals; Ramanathan-Girish *et al.*, 2004) and LBM-415 (VIC-104959; Novartis Pharmaceuticals; Leeds & Dean, 2006; Fig. 1). These inhibitors have shown strong antibacterial activity against a wide range of pathogens, particularly Gram-positive aerobes and some Gram-negative anaerobes (Guay, 2007). *S. aureus* and *K. pneumoniae* are the main causes of hospital- and community-acquired infections. Moreover, high frequencies of methicillin-resistant and vancomycin-resistant *S. aureus*, as well as ceftazidime/ceftriaxone-resistant *K. pneumoniae*, pose serious health problems (Boucher & Corey, 2008; Klevens *et al.*, 2006; Rosenthal *et al.*, 2009).

Human PDF has an approximate sequence identity of 28–34% to bacterial PDFs. The unexpected finding of a human mitochondrial peptide deformylase has apparently not dampened enthusiasm for this potential new class of antibacterials. Furthermore, the lack of reported toxicity to human and other animal cells, despite evident antibacterial

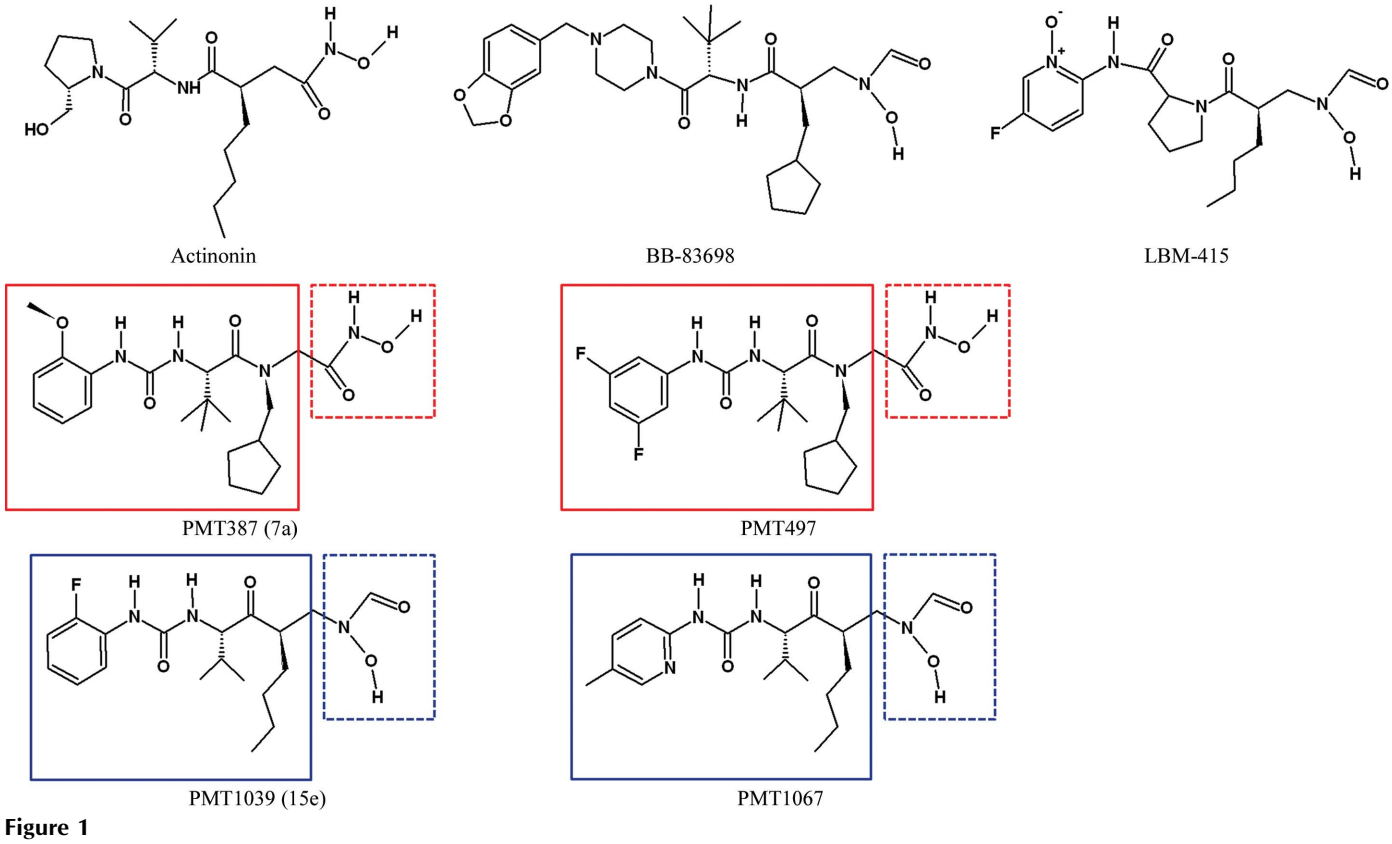

Figure 1
Peptide-scaffold hydroxamate inhibitors [PMT387 (7a) and PMT497] and nonpeptide-scaffold reverse-hydroxamate inhibitors [PMT1039 (15e) and PMT1067]. The peptide-scaffold and hydroxamate moieties of PMT387 (7a) and PMT497 are indicated by red lines and red dashes, respectively. The nonpeptide scaffolds and reverse-hydroxamate moieties of PMT1039 (15e) and PMT1067 are indicated by blue lines and blue dashes, respectively.

Table 1
Results of enzymatic assays and MICs.

		MIC (mg ml^{-1})						
		S. aureus (ATCC 6538p)	*K. pneumoniae* (ATCC 10031)	*E. coli* (ATCC 25922)	*S. pneumoniae* (ATCC 6305)	*M. catarrhalis* (ATCC 43617)	*H. influenzae* (ATCC 49247)	*P. aeruginosa* (ATCC 27853)
Inhibitor	K_i (n*M*)	Gram-positive	Gram-negative	Gram-negative	Gram-positive	Gram-negative	Gram-negative	Gram-negative
PMT387 (7a)†	84.9 ± 12.8	50	0.4–0.8	25	0.2‡	0.1‡	0.2‡	100
PMT497	52.4 ± 6.5	50	6.3	25	0.8	0.1	0.1	200
PMT1039 (15e)†	35.1 ± 3.1	0.2‡	0.1	12.5	0.1–0.2‡§	0.1‡	0.1‡	200
PMT1067	11.2 ± 1.6	0.2	0.4	12.5	0.1‡	0.4	0.1	200
Actinonin	319.2 ± 39.3	6.3–12.5	0.8–3.2	25–50	3.2–6.3	0.1–0.2	1.6–3.2	100–200
Ampicillin	No data	0.2	25–100	1.6	0.1	0.1–0.4	3.2	200
LBM-415¶	No data	2	32	32	1	0.5	4–8	N.A.

† The nomenclature in parentheses was used in previous reports (Lee *et al.*, 2010, 2011). ‡ The results of antibacterial inhibition assays have been described in previous reports (Lee *et al.*, 2010, 2011). § Antibacterial inhibition assays were performed on both strains of *S. pneumoniae* (ATCC 6305 and ATCC 49619). ¶ The inhibition-assay data were taken from Credito *et al.* (2004), Fritsche *et al.* (2005) and Watters *et al.* (2006).

action, has indicated that the human mitochondrial PDF protein may not be functional or that the tested inhibitors may not reach the mitochondrion (Nguyen *et al.*, 2003; Robien *et al.*, 2004). The inhibitors of human PDF have been reported to be potent anticancer drugs that promote cell death or proliferation arrest in a wide variety of cancer cell lines (Grujic *et al.*, 2005; Lee *et al.*, 2004; Xu *et al.*, 1998). Interestingly, it has been reported that actinonin prevents bacterial survival and has a considerable influence on innate immune reactions in humans (Fu *et al.*, 2006; Mader *et al.*, 2010). Such pro-inflammatory consequences can be beneficial for the host and serve to clear localized infections (Mader *et al.*, 2010). Moreover, all of the resistant mutants have a slow-growth phenotype similar to that of the the *fmt*/*def* double-knockout mutants, which are less virulent than the PDF-inhibitor-sensitive parental strains (Apfel *et al.*, 2000; Margolis *et al.*, 2000; Watters *et al.*, 2006). These studies show the considerable promise of bacterial PDF as a novel antibacterial drug candidate.

Presently, only one crystal structure of inhibitor-bound *S. aureus* PDF complexed with actinonin is available (Yoon *et al.*, 2004). In this study, we have performed structural analysis of *S. aureus* PDF complexed with the hydroxamate/pseudopeptide inhibitors PMT387 (7a) and PMT497 and the reverse-hydroxamate/nonpeptide scaffold compounds PMT1039 (15e) and PMT1067 at resolutions of 1.90–2.30 Å, which provided a detailed atomic level view of the binding modes of the PDF inhibitors (Fig. 1). These PDF inhibitors were highly effective against infectious respiratory-tract pathogens, including *S. pneumoniae*, *M. catarrhalis* and *H. influenza*, as well as leading nosocomial pathogens such as *S. aureus* and *K. pneumoniae*. Of these inhibitors, PMT1039 (15e) and PMT1067, with nonpeptide scaffolds, were highly effective in inhibiting the *S. aureus* and *K. pneumoniae* PDFs.

When we compared and analyzed the four new inhibitor-bound PDF structures, distinct structural changes that were dependent on the inhibitor class were observed. The structural changes appear to be driven by the binding of the inhibitor and are likely to be involved in inhibition, particularly of *S. aureus*.

2. Materials and methods

2.1. Measurement of PDF activity

The PDF activity of *S. aureus* PDF was determined. Recombinant *S. aureus* PDF with a C-terminal hexahistidine-containing tag was expressed and purified. The purification procedures were identical to those used for the production of crystals except for the cell-disruption procedure. The wet cells were homogenized with a Dounce glass homogenizer (100 ml size) on ice instead of sonication. For the assay, 50 µl of a reaction mixture consisting of 50 m*M* HEPES pH 7.0, 10 m*M* NaCl, 0.1% Triton X-100 was used. Assays were performed for 10 min at 303 K with an inhibitor concentration in the range 0.001–100 µ*M* and 500 n*M* *S. aureus* PDF. The reaction was initiated by the addition of substrate (50 µl 5 m*M* formyl-Met-Ala-Ser; Bachem). The formation of the product was detected using fluorescamine. For the assay, 50 µl 150 µg ml^{-1} fluorescamine and 50 µl 50 m*M* borate–sodium hydroxide buffer pH 9.5 were added. The fluorescence was quantified with a Gemini EM Spectrofluorometer Microplate Reader (Molecular Devices) using an excitation wavelength of 390 nm and an emission wavelength of 465 nm. The K_i values of the inhibitors were calculated using *GraphPad Prism* (GraphPad Software). Protein concentrations were determined using the Bradford method with bovine serum albumin as a standard (Bradford, 1976). Enzymatic assay results are presented in Table 1.

2.2. Bacteria, reagents and miminal inhibitory concentration (MIC) tests

S. aureus (ATCC 6538p), *K. pneumoniae* (ATCC 10031), *E. coli* (ATCC 25922), *S. pneumoniae* (ATCC 6305 and ATCC 49619), *M. catarrhalis* (ATCC 43617), *H. influenzae* (ATCC 51907) and *P. aeruginosa* (ATCC 27853) were tested using *in vitro* susceptibility tests (MIC). *S. aureus*, *K. pneumoniae*, *E. coli* and *P. aeruginosa* were cultured in Mueller Hinton broth (Oxoid) at 310 K for 24 h. *S. pneumoniae* was cultured in tryptic soy broth (Difco) with 5% sheep blood at 310 K for 48 h in a 5% CO_2 incubator. *M. catarrhalis* and *H. influenzae* were grown in brain–heart infusion broth (Difco) supple-

Table 2
Data-collection and model-refinement statistics.

Values in parentheses are for the highest resolution shell.

Data set	PMT387 (7a)†	PMT497	PMT1039 (15e)†	PMT1067
Data collection				
X-ray wavelength (Å)	0.9722	0.9722	1.0000	1.0000
Space group	$C222_1$	$C222_1$	$C222_1$	$C222_1$
Unit-cell parameters (Å)				
a	93.77	94.78	94.58	93.75
b	120.27	120.21	119.70	120.65
c	47.75	47.79	47.27	47.56
Resolution range (Å)	20–1.9 (1.97–1.90)	50–2.0 (2.07–2.0)	20–2.15 (2.23–2.15)	20–2.3 (2.38–2.30)
Total/unique reflections	127541/21933	96279/18445	110518/14864	67943/12218
Completeness (%)	99.5 (99.9)	99.7 (100)	99.4 (94.3)	98.6 (96.0)
$\langle I/\sigma(I)\rangle$	22.2 (4.0)	20.9 (4.3)	53.4 (13.9)	30.6 (7.1)
$R_{\rm merge}$‡	0.167 (0.496)	0.116 (0.469)	0.055 (0.164)	0.090 (0.190)
Model refinement				
$R_{\rm work}/R_{\rm free}$§	0.216/0.266	0.208/0.235	0.196/0.223	0.195/0.228
No. of non-H atoms/average *B* factor (Å^2)				
Protein atoms	1462/16.6	1462 22.0	1462/27.1	1462/32.4
Water O atoms	202/28.5	121/29.3	113/35.0	94/37.0
Inhibitor	31/23.2	31/32.9	27/57.9	27/58.8
Wilson *B* factor (Å^2)	26.2	31.2	39.4	46.3
R.m.s.d.s from ideal geometry				
Bond lengths (Å)	0.011	0.010	0.009	0.010
Bond angles (°)	1.33	1.36	1.37	1.23
R.m.s. *Z* scores¶				
Bond lengths	0.452	0.421	0.379	0.427
Bond angles	0.562	0.554	0.563	0.524
Ramachandran plot†† (%)				
Favoured	99.5	100.0	98.9	99.5
Outliers	0.0	0.0	0.0	0.0
Rotamer outliers†† (%)	0.63	0.63	0.63	0.0

† The nomenclature in parentheses was used in previous reports (Lee *et al.*, 2010, 2011). ‡ $R_{\rm merge} = \sum_{hkl}\sum_i |I_i(hkl) - \langle I(hkl)\rangle|/\sum_{hkl}\sum_i I_i(hkl)$, where $I(hkl)$ is the intensity of reflection hkl, $\sum_{hkl}$ is the sum over all reflections and $\sum_i$ is the sum over i measurements of reflection hkl. § $R = \sum_{hkl}\big||F_{\rm obs}| - |F_{\rm calc}|\big|/\sum_{hkl}|F_{\rm obs}|$; $R_{\rm free}$ is calculated for a randomly selected set of 5% of the reflections which were not used for structure refinement and $R_{\rm work}$ is calculated for the remaining reflections. ¶ Values obtained using *REFMAC* (Murshudov *et al.*, 2011). †† Values obtained using *MolProbity* (Chen *et al.*, 2010).

mented with 2.5% horse serum, 10 mg NAD^+ and 5 mg haemin per litre for 24 and 48 h, respectively, in a 5% CO_2 incubator. All bacterial strains were obtained from the American Type Culture Collection. Ampicillin, an antibacterial agent used as a control, was purchased from Sigma–Aldrich (USA). The inhibitor compounds [PMT387 (7a), PMT497, PMT1039 (15e), PMT1067 and actinonin] were synthesized as described previously (Lee *et al.*, 2010, 2011). Other compounds were obtained from their respective manufacturers. MIC tests were performed using the Clinical and Laboratory Standards Institute (CLSI, formerly NCCLS) broth microplate method (National Committee for Clinical Laboratory Standards, 2003), with a starting inoculum of approximately 10^6 CFU ml^{-1} for all isolates. The MIC was defined as the lowest concentration of antimicrobial agent that inhibited visible growth. The results of the MIC tests are summarized in Table 1.

2.3. Protein purification and crystallization

The *def* (*SACOL1100*) gene from *S. aureus* COL was amplified by polymerase chain reaction using the genomic DNA as the template. The forward and reverse oligonucleotide primers were designed using the published genome sequence (Gill *et al.*, 2005) and were 5′-G GAA TTC **CAT ATG** TTA ACA ATG AAA GAC ATC ATT AGC G-3′ and 5′-CCG CCG **CTC GAG** AAC TTC TAC TGC ATC TGT ATG TGG-3′, respectively. The sequences in bold are *Nde*I and *Xho*I restriction-enzyme sites, respectively. The recombinant protein sequence contained an eight-residue tag (LEHHHHHH) that was added to the carboxy-terminus of the recombinant protein. The gene was cloned into the pET-21a(+) expression vector (Novagen). Recombinant protein with a C-terminal hexahistidine-containing tag was overexpressed in *E. coli* C41 (DE3) cells in Terrific Broth. Protein expression was induced by the addition of 0.5 m*M* isopropyl β-D-1-thiogalactopyranoside and the cells were incubated for an additional 20 h at 303 K following growth to mid-log phase at 310 K. The cells were lysed by sonication in buffer *A* (20 m*M* Tris–HCl pH 7.9, 50 m*M* imidazole, 500 m*M* NaCl) containing 10%(*v*/*v*) glycerol. The crude lysate was centrifuged at approximately 36 000*g* for 60 min. The supernatant was applied onto a HiTrap Chelating HP affinity chromatography column (GE Healthcare) which was equilibrated with buffer *A*. After elution with a gradient of imidazole in buffer *A*, the protein was further purified by gel filtration on a Superdex 200 prep-grade column (GE Healthcare) which was equilibrated with 20 m*M* Tris–HCl buffer pH 7.5 containing

120 m*M* NaCl. For crystallization, the fractions containing *S. aureus* PDF were concentrated to 30 mg ml^{-1} using an Amicon Ultra-15 centrifugal filter unit (Millipore).

To grow crystals of the protein–inhibitor complexes, the protein solution was incubated at 297 K for 1 h with the inhibitors, which were dissolved in a 6.6-fold molar excess of dimethyl sulfoxide. The crystals were grown by the hanging-drop vapour-diffusion method at 297 K by mixing equal volumes (2 µl each) of protein solution (30 mg ml^{-1} concentration in 20 m*M* Tris–HCl buffer pH 7.5 containing 120 m*M* NaCl) and reservoir solution consisting of 23%(*w*/*v*) PEG 4000, 50 m*M* Tris–HCl pH 8.5, 15%(*v*/*v*) glycerol, 100 m*M* $MgCl_2$, 20 m*M* $CaCl_2$. The crystals grew to approximate dimensions of 0.04 × 0.02 × 0.4 mm within one week.

2.4. X-ray data collection, structure determination and refinement

X-ray diffraction data were collected at 100 K using an ADSC Quantum 4R CCD detector on beamline BL-38B1 at SPring-8 (λ = 0.9722 Å), Japan or an ADSC Quantum 315 CCD detector system on beamline BL-5A at Photon Factory (λ = 1.0000 Å), Japan. The crystal was rotated by 1° for each image and the raw data were processed and scaled using the *HKL*-2000 program suite (Otwinowski & Minor, 1997). The crystals belonged to the orthorhombic space group $C222_1$. One monomer was present in each asymmetric unit of the crystal.

The structures of *S. aureus* PDF in complex with four inhibitors were determined by molecular replacement using the program *MOLREP* (Vagin & Teplyakov, 2010). A model of *S. aureus* PDF (Yoon *et al.*, 2004) was used as a search model. In addition, 5% of the data were randomly set aside as a test set for calculating $R_{\rm free}$ (Brünger, 1992). The models were built manually using the program *Coot* (Emsley *et al.*, 2010) and refined with the program *REFMAC* (Murshudov *et al.*, 2011), including bulk-solvent correction. The inhibitors [PMT387 (7a), PMT497, PMT1039 (15e) and PMT1067] and water molecules were assigned according to $mF_{\rm o} - DF_{\rm c}$ maps calculated with the model phases. Inhibitor and water molecules were added using *Coot* and were manually inspected. All of the models presented excellent stereochemistry, which was evaluated using the program *MolProbity* (Chen *et al.*, 2010). Structural deviation was calculated using *SUPERPOSE* (Krissinel & Henrick, 2004). The refinement statistics are summarized in Table 2. The atomic coordinates and structure factors of *S. aureus* PDF in complex with the four new inhibitors [PMT387 (7a), PMT497, PMT1039 (15e) and PMT1067] have been deposited in the Protein Data Bank and their PDB codes are listed in Table 2.

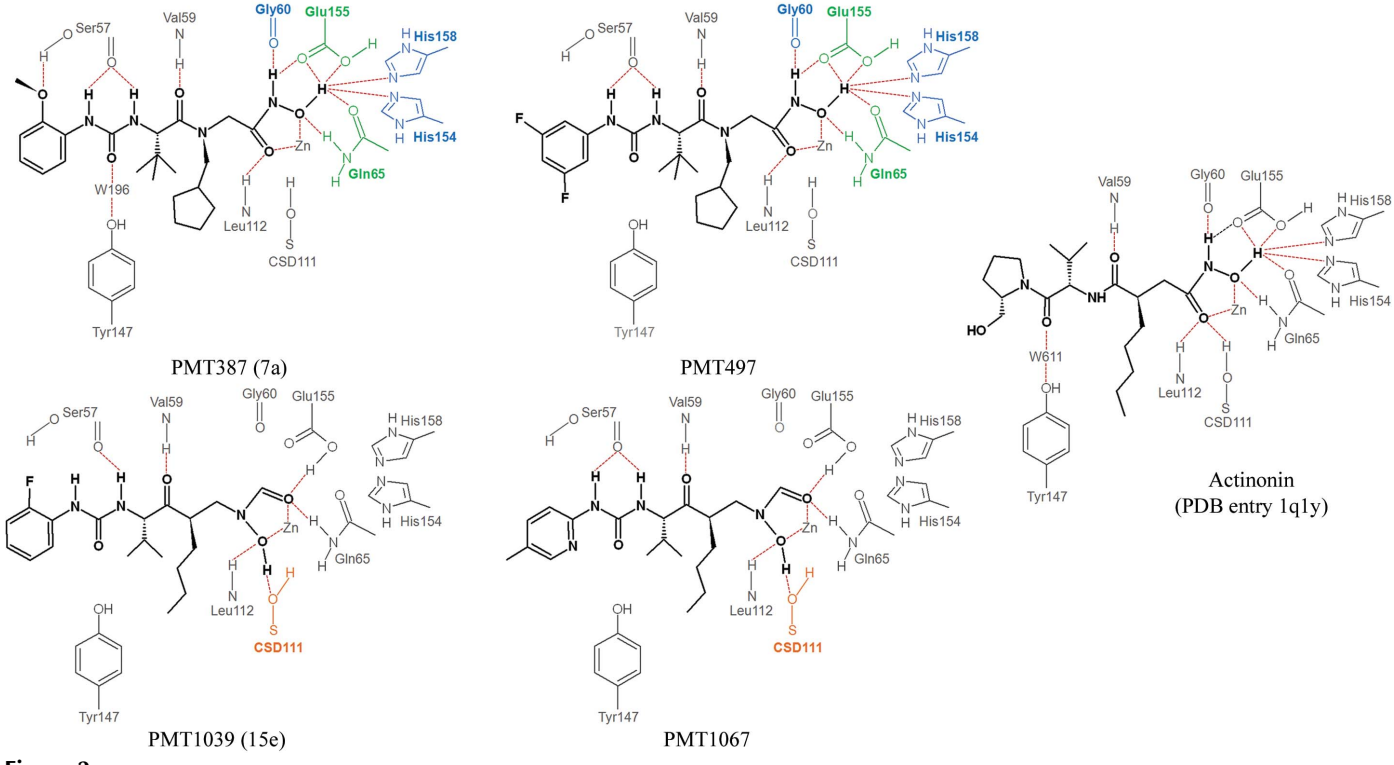

Figure 2
The binding modes of PMT387 (7a), PMT497, PMT1039 (15e), PMT1067 and actinonin (PDB entry 1q1y) to the active site of *S. aureus* PDF. The intermolecular interactions and inhibitor–Zn^{2+} ion interactions are depicted. The residues binding to PMT387 (7a), PMT497, PMT1039 (15e), PMT1067 and actinonin are coloured blue, green, orange and grey according to the inhibitor-class binding characteristics. The binding residues that only interact with peptide-scaffold hydroxamate inhibitors are coloured blue. The binding residues that only interact with nonpeptide scaffold reverse hydroxamate inhibitors are coloured orange. Green residues indicate interactions with both classes; however, more interactions were observed with peptide-scaffold hydroxamate inhibitors. The residues with similar interactions or no characteristics are coloured grey. Intermolecular interactions are designated by red dashes.

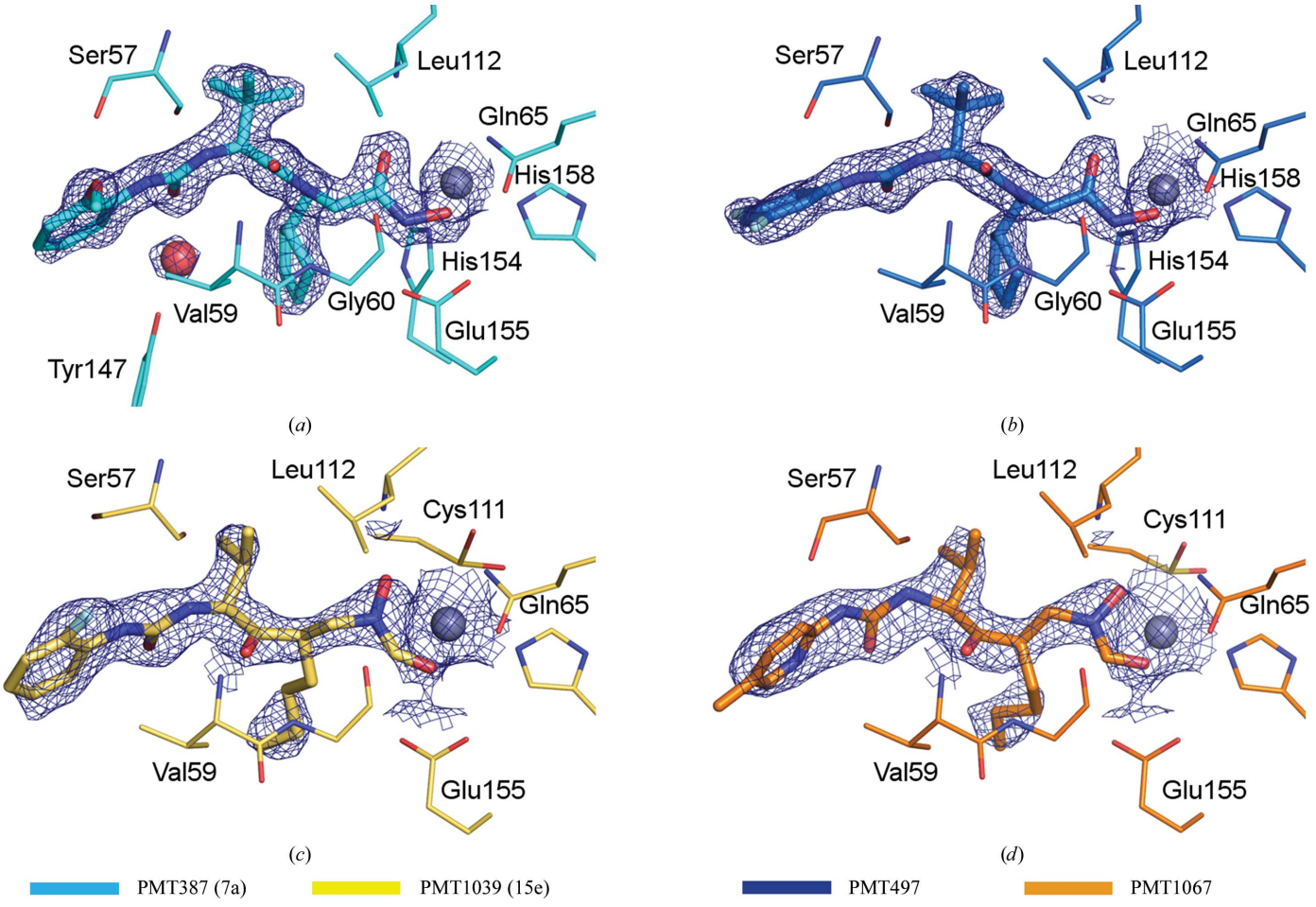

Figure 3
$2mF_o - DF_c$ electron-density map (coloured blue and contoured at 1.2σ) of PMT387 (7a), PMT497, PMT1039 (15e) and PMT1067. A Zn^{2+} ion and a water molecule (W196) are depicted as spheres and are coloured purple and red, respectively. The figures were drawn using *PyMOL* (DeLano, 2002).

3. Results and discussion

3.1. Antibacterial activities of the four inhibitors

In our exploration of inhibitors of PDFs, our structure–activity relationship study of retro-amide PDF inhibitors led us to discover PMT387 (7a) and PMT497, which enabled us to develop the nonpeptide and reverse-hydroxamate inhibitors PMT1039 (15e) and PMT1067 (Lee *et al.*, 2010, 2011). The inhibitors used in this study are categorized into two types: peptide scaffolds [PMT387 (7a) and PMT497] and nonpeptide scaffolds [PMT1039 (15e) and PMT1067] (Fig. 1). The K_i values for inhibition of *S. aureus* PDF by the four compounds PMT387 (7a), PMT497, PMT1039 (15e) and PMT1067 were measured as 84.9 ± 12.8, 52.4 ± 6.5, 35.1 ± 3.1 and 11.2 ± 1.6 n*M*, respectively (Table 1). The reverse-hydroxamate/nonpeptide compounds [PMT1039 (15e) and PMT1067] were found to have a higher binding affinity for *S. aureus* PDF than the hydroxamate/pseudopeptide compounds [PMT387 (7a) and PMT497].

When we tested the four inhibitors PMT387 (7a), PMT497, PMT1039 (15e) and PMT1067 against *S. aureus*, *K. pneumoniae*, *E. coli*, *S. pneumoniae*, *M. catarrhalis* and *H. influenzae*, all four inhibitors had MICs of between 0.1 and 0.8 mg ml^{-1} for the pathogens that are related to respiratory-tract infections (*S. pneumoniae*, *M. catarrhalis* and *H. influenzae*; Table 1). Interestingly, although the four inhibitors exhibited very similar MICs for pathogens related to respiratory-tract infections, PMT1039 (15e) and PMT1067 presented superior inhibition activities against *S. aureus* compared with PMT387 (7a) and PMT497, with MICs of 0.2 mg ml^{-1}. The antimicrobial activities of PMT1039 (15e) and PMT1067 against *S. aureus* were 250-fold higher than those of PMT387 (7a) and PMT497. Therefore, the critical issue of the optimization of these compounds can be emphasized by understanding the limited correlation between enzymatic inhibition and MIC data, as well as by understanding the molecular interactions with PDF. The detailed assay data are summarized in Table 1.

3.2. Structure determination and model quality of inhibitor-bound *S. aureus* PDF

The four refined inhibitor-bound *S. aureus* PDF models contained 183 amino-acid residues in the monomer, a Zn^{2+} ion and 75–201 water molecules in the asymmetric unit. The structures with PMT387 (7a), PMT497, PMT1039 (15e) and

PMT1067 had R_{work}/R_{free} values of 0.216/0.266, 0.208/0.235, 0.196/0.223 and 0.195/0.228 for the resolution ranges 20–1.9, 50–2.0, 20–2.15 and 20–2.3 Å, respectively. In these four models, the six histidine residues in the C-terminal fusion tag were disordered. The four inhibitor-bound structures of *S. aureus* PDF were highly similar to each other and had r.m.s. deviations (r.m.s.d.s) of 0.08–0.20 Å for 183 C^{α}-atom pairs. The OMIT map around Cys111 clearly shows that the functional sulfhydryl group of Cys111 in the active site is oxidized to sulfinic acid (Cys-SO_2H; Supplementary Fig. S1[1]) and this observation is in good agreement with previous studies of PDFs from *S. aureus*, *S. pneumoniae* and *Thermotoga maritima*, in which the corresponding Cys residue is found in the form of sulfinic acid/sulfonic acid (Kreusch *et al.*, 2003; Yoon *et al.*, 2004). Although it remains unclear how the oxidation of Cys111 can be achieved under the reducing conditions of the physiological environment in the bacterial cell, it is possible that the oxidation is caused by superoxide radical or another unidentified reactive species (Rajagopalan & Pei, 1998). More extensive studies are required to elucidate the biological relevance of cysteine oxidation.

3.3. Structures of *S. aureus* PDF bound to four different inhibitors

The structures of *S. aureus* PDF bound to four different inhibitors [PMT387 (7a), PMT497, PMT1039 (15e) and PMT1067] and an actinonin-bound PDF structure (PDB entry 1q1y; Yoon *et al.*, 2004) were compared with an inhibitor-free structure (PDB code 1lmh; Baldwin *et al.*, 2002).

In PMT387 (7a)-bound *S. aureus* PDF the hydroxamate and peptide-scaffold moieties of PMT387 (7a) are recognized by residues Gly60/Gln65/Leu112/Glu155/His154/His158/Zn^{2+} and Ser57/Val59/Tyr147, respectively (Figs. 2 and 3). PMT497 is bound to the active site in a highly similar manner to PMT387 (7a). However, PMT497 does not interact with either Tyr147 or the side chain of Ser57 in *S. aureus* PDF, unlike PMT387 (7a) (Figs. 2 and 3). The binding modes of PMT387 (7a) and PMT497 are similar to that of actinonin. Actinonin makes an additional interaction with Cys111, whereas it does not interact with Ser57. A unique feature of the PMT387 (7a)-bound and PMT497-bound structures is the carbonyl oxygen–Zn^{2+} ion and hydroxyl oxygen–Zn^{2+} ion distances in the hydroxamate moieties (Fig. 3). Unlike actinonin, which has a symmetric geometry between two O atoms and the Zn^{2+} ion (2.4 and 2.4 Å), PMT387 (7a) and PMT497 present distorted geometries, with carbonyl oxygen–Zn^{2+} ion distances of 3.0 and 3.1 Å and hydroxyl oxygen–Zn^{2+} ion distances of 2.1 and 2.2 Å, respectively. The reverse-hydroxamate nonpeptide inhibitors PMT1039 (15e) and PMT1067 share similar binding modes. However, fewer interactions were observed compared with PMT387 (7a) and PMT497. In PMT1039 (15e)-bound *S. aureus* PDF, the reverse-hydroxamate and nonpeptide scaffold moieties of PMT1039 (15e) were recognized by residues Gln65/Cys111/Leu112/Glu155/Zn^{2+} and Ser57/Val59, respectively (Figs. 2 and 3). PMT1067 is bound to the active site in a manner highly similar to PMT1039 (15e), apart from an interaction with Ser57 (Figs. 2 and 3). Unlike PMT1039 (15e), two N atoms in the peptide-scaffold moiety of PMT1067 were shown to interact with Ser57. These two reverse-hydroxamate nonpeptide inhibitors [PMT1039 (15e) and PMT1067] have an isosceles-geometry bonding mode between the hydroxyl O atom and the Zn^{2+} ion and between the carbonyl O atom and the Zn^{2+} ion in the reverse-hydroxamate moieties. The distances between the two O atoms and Zn^{2+} are 2.8 and 2.7 Å in the PMT1039 (15e) complex and 2.4 and 2.5 Å in the PMT1067 complex.

Like the other PDFs, *S. aureus* PDF has three inhibitor-interacting regions (S1′, S2′ and S3′) along with a metal-binding site that forms a deep cleft. The substituents (P1′, P2′ and P3′) of the four inhibitors corresponding to the three binding pockets are shown in Fig. 4. The structural features of the P1′, P2′ and P3′ components of the inhibitors correspond to the density observed in the four inhibitor-bound *S. aureus* PDF structures (Fig. 4). The S1′ region of *S. aureus* PDF is composed of residues Gly60, Leu105, Gly108, Glu109, Ile150, Val151, His154 and Glu155. The substituents in P1′ are a cyclopentylmethyl group [in PMT387 (7a) and PMT497] or a butylmethyl group [in PMT1039 (15e) and PMT1067]. Our previous study showed that the size of the substituent at P1′ affects the antimicrobial activity (Lee *et al.*, 2010). The *n*-pentyl chain and cyclopentylethyl group were slightly long for the S1′ cavity of *S. aureus* PDF and presented reduced

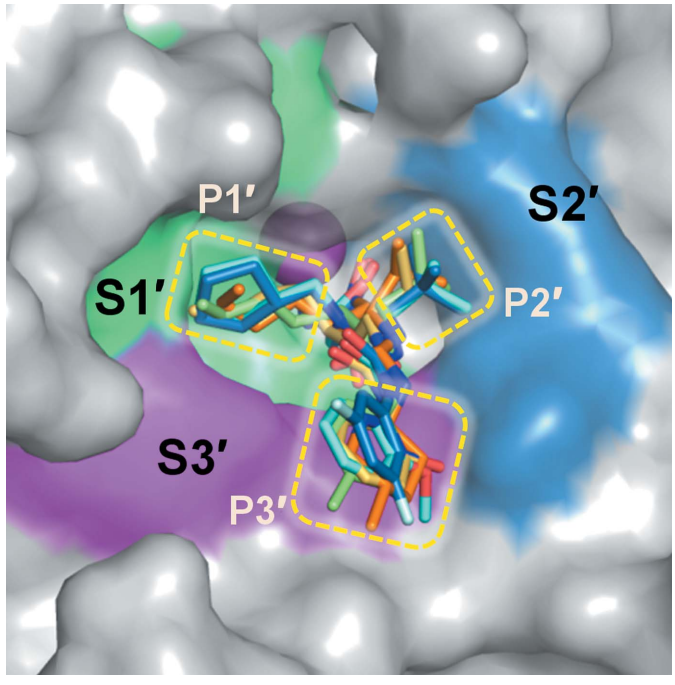

Figure 4
Surface diagram of *S. aureus* PDF with the active-site pocket depicted. The four inhibitors are also shown. The molecular surface is coloured green (S1′), blue (S2′) and magenta (S3′). The P1′, P2′ and P3′ residues of the four inhibitors corresponding to the S1′, S2′ and S3′ sites are indicated by yellow dashes. The Zn^{2+} ion is shown as a sphere.

[1] Supplementary material has been deposited in the IUCr electronic archive (Reference: MH5056). Services for accessing this material are described at the back of the journal.

activity. Cyclopropylmethyl and cyclobutylmethyl groups had a reduced inhibitory effect on bacterial growth.

These compounds do not fit into the S1′ pocket very well. Accordingly, we screened and selected cyclopentylmethyl for PMT387 (7a) and PMT497 and butylmethyl for PMT1039 (15e) and PMT1067. This is in agreement with our previous reports (Lee *et al.*, 2010, 2011) concerning inhibitor-bound structures.

The S2′ region of *S. aureus* PDF is composed of residues Arg56, Cys111 and Leu112. The P2′ region, which corresponds to S2′, was optimized as *t*-leucine [in PMT387 (7a) and PMT497] or valine [in PMT1039 (15e) and PMT1067]. The size and length of the substituents in the P2′ region have significant effects on the antimicrobial activity, especially against *S. aureus* (Lee *et al.*, 2011). These effects arise from the size of the S2′ region, which is not wider than the S1′ region. In the case of PMT387 (7a) and PMT497, a shorter or longer side chain than valine was shown to reduce the antimicrobial activity, which led to the discovery of *t*-leucine as the optimal residue for inhibiting the growth of bacteria. Therefore, when the side chain was *t*-leucine the antimicrobial activity of the reverse-hydroxamate nonpeptide inhibitors against *S. aureus* PDF was significantly reduced. This result allowed us to select valine as an effective P2′ substituent in the development of the reverse-hydroxamate nonpeptide inhibitors (Lee *et al.*, 2011).

The S3′ region of *S. aureus* PDF is composed of residues Ser57, Gly58, Val59 and Tyr147. Our intensive search for P3′ substituents led us to discover a 2-methoxyphenyl ring [PMT387 (7a)] and a 3,5-difluorophenyl ring, both of which significantly increased antimicrobial activity against the tested

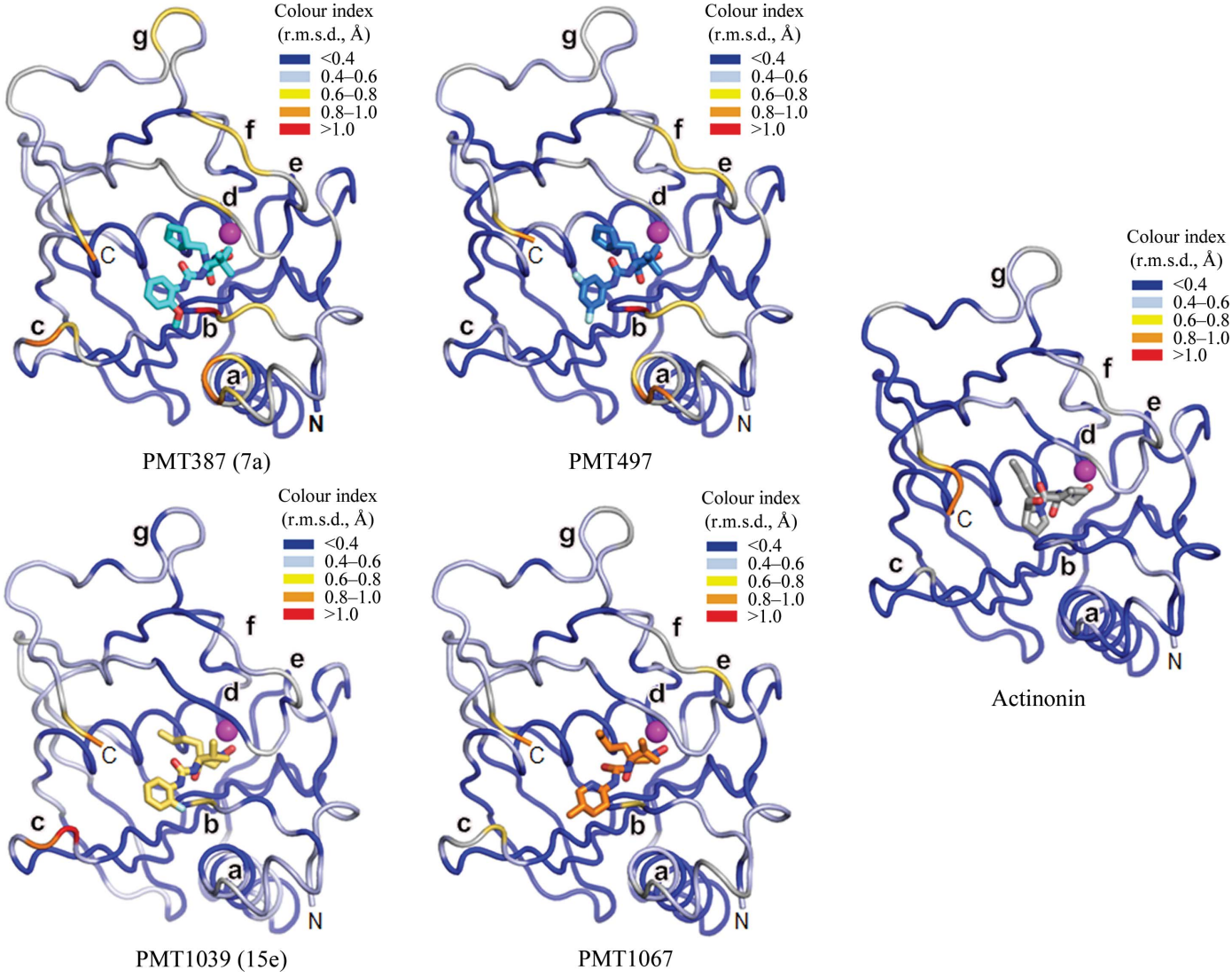

Figure 5
Structural changes arising from the effects of inhibitors binding to *S. aureus* PDF. Residues are coloured using a linear ramp from blue for unperturbed structures (r.m.s.d. < 0.4 Å) to red for perturbations greater than an r.m.s.d. of 1.0 Å. Residues shown in blue exhibited no measurable change in r.m.s.d., while red residues were more flexible in the complex structures. Residues 41–51, 54–58, 80–81, 107–110, 115–116, 117–120 and 171–175 are indicated by a, b, c, d, e, f and g, respectively. The Zn^{2+} ion is shown as a magenta sphere and the five inhibitors (including actinonin) are shown as sticks with atoms coloured by type.

strains (Lee *et al.*, 2010). For the reverse-hydroxamate nonpeptide inhibitors, a 2-fluorophenyl ring [PMT1039 (15e)] substitution was shown to have the most potent activity and 3-methylpiperidine (PMT1067) was also effective (Lee *et al.*, 2010, 2011; Table 1).

3.4. Effects of inhibitors on the structure of *S. aureus* PDF

There were measurable structural differences between the four inhibitor-bound *S. aureus* PDF structures and an inhibitor-free structure. Therefore, we hypothesized that induced-fit recognition may play a role in inhibitor binding. To obtain structural insights into the role of protein flexibility in molecular recognition, we plotted the r.m.s.d.s of five separate structures of *S. aureus* PDF bound to five inhibitors (including actinonin) and compared the structures with the inhibitor-free structure (Fig. 5). Interestingly, the structural comparisons indicated that the structure of *S. aureus* PDF undergoes a small conformational change that depends on the type of inhibitor: hydroxamate pseudopeptide inhibitors [PMT387 (7a) and PMT497] or reverse-hydroxamate nonpeptide inhibitors [PMT1039 (15e) and PMT1067]. The key findings are summarized in Fig. 5 and Supplementary Fig. S2. Residues 41–51 (corresponding to S3′), 54–58 (corresponding to S2′), 107–110 (corresponding to S1′), 117–120 and 171–175 present greater deviations in the PMT387 (7a)- and PMT497-bound PDF structures compared with structures in which PDF was bound to the two reverse-hydroxamate nonpeptide inhibitors PMT1039 (15e) and PMT1067 or actinonin (PDB entry 1q1y). The two reverse-hydroxamate inhibitor-bound PDF structures present greater deviations of residues 115–116. For residues 80–81 (corresponding to S2′), the PMT387 (7a)- and PMT1039 (15e)-bound PDF structures present greater deviations. Residues 41–51, 54–58 and 107–110 are located in the active site. In the case of the hydroxamate peptide inhibitors, deviations of residues 41–51, 54–58 and 107–110 were found. In addition to the affected residues 107–110 mentioned above, their flanking residues 115–120 as well as the neighbouring residues 171–175 also showed concurrent structural changes. The structural rearrangements induced by the hydroxamate peptide inhibitors involved local changes in the active-site pocket and global structural changes transmitted *via* interaction networks to other parts of the protein, while the reverse-hydroxamate nonpeptide inhibitors were not shown to have such effects on conformational change. These ligand–enzyme complexes cause a specific structural perturbation that affects regions remote from the active site. These results are in agreement with previous findings that indicated that local entropy changes in an active site can be redistributed from one site to another in a protein, which has important thermodynamic implications (Amero *et al.*, 2009).

The structure of PDF is rigid in the absence of ligands, in contrast to other members of the metallohydrolase superfamily (Amero *et al.*, 2009; Moy *et al.*, 2002). This lack of flexibility may be related to the narrow specificity of PDF for substrates that are peptides bearing N-formylated methionine residues (Amero *et al.*, 2009; Hu *et al.*, 1999; Ragusa *et al.*, 1999). Despite the high rigidity of the *S. aureus* structure, two different classes of PDF inhibitors induced local structural changes. We observed that these structures displayed distinct structural features depending on the inhibitor class. The distances between the hydroxamate carbonyl O atom and the Zn^{2+} ion and between the reverse-hydroxamate hydroxyl O atom and the Zn^{2+} ion in the hydroxamate or reverse-hydroxamate moiety appeared to be correlated with selective and strong inhibition activity against *S. aureus* (Table 1). When we compared the two classes of inhibitor-bound structures, a distinctive change in the *S. aureus* PDF structure was also observed which was driven by the binding of specific inhibitors. As shown in Fig. 2, the binding modes of the inhibitors demonstrate comparable characteristics that were dependent on the inhibitor class. These structural changes appear to be involved in the inhibition activity against *S. aureus*.

Most known PDF inhibitors consist of a hydroxamate moiety and a pseudopeptide backbone. Although a hydroxamate compound such as actinonin is regarded as an extremely effective inhibitor, such a compound typically displays poor selectivity by chelating the metals of other metalloproteins that are cytotoxic to mammalian cells and also shows poor oral bioavailability related to characteristic rapid metabolization (Aubart & Zalacain, 2006; Antczak *et al.*, 2011; Fisher & Mobashery, 2006). In terms of resolving the problems of poor selectivity as well as oral bioavailability, the use of either a reverse-hydroxamate moiety or a nonpeptide backbone may be considered to be one alternative method of improving current PDF inhibitors. The study that we present here provides new structural information on four inhibitor complexes of *S. aureus* PDF which will aid in the design of new potential inhibitors and will provide important data for selective antimicrobial strategies. Further studies combining structural (X-ray crystallographic or nuclear magnetic resonance) evidence from PDFs from other strains or different types of enzymes will aid in improving rational drug design. The binding of an inhibitor to an enzyme is more complex than is generally assumed; therefore, we suggest that accurate information on local and long-range contributions to molecular behaviour will be required for the rational design of an inhibitor, especially for antibacterial drugs.

We thank the beamline staff at the Photon Factory (BL-5A) and SPring-8 (BL38-B1), Japan for assistance in the X-ray diffraction experiments. This work was partially supported by the Innovative Drug Research Center for Metabolic and Inflammatory Disease, Basic Science Outstanding Scholars Program, World-Class University Program and Korea Healthcare Technology R&D Project, Ministry for Health, Welfare and Family Affairs, Republic of Korea (grant No. A092006) (SWS) and the Mid-career Researcher Program (2011-0029294) and the Bio and Medical Technology Development Program (2011-0030032) through the National Research Foundation of Korea (NRF) and funded by the Ministry of Education, Science and Technology and National

Cancer Center Research Grant (grant No. 1110012) (BIL). S-JL is a Howard Hughes Medical Institute postdoctoral fellow. SJL is supported by funding from the Fostering Next-Generation Researchers program, which was granted by NRF, Republic of Korea (NRF-2011-355-C00118).

References

Amero, C. D., Byerly, D. W., McElroy, C. A., Simmons, A. & Foster, M. P. (2009). *Biochemistry*, **48**, 7595–7607.

Antczak, C., Shum, D., Bassit, B., Frattini, M. G., Li, Y., de Stanchina, E., Scheinberg, D. A. & Djaballah, H. (2011). *Bioorg. Med. Chem. Lett.* **21**, 4528–4532.

Apfel, C., Banner, D. W., Bur, D., Dietz, M., Hirata, T., Hubschwerlen, C., Locher, H., Page, M. G., Pirson, W., Rossé, G. & Specklin, J. L. (2000). *J. Med. Chem.* **43**, 2324–2331.

Aubart, K. & Zalacain, M. (2006). *Prog. Med. Chem.* **44**, 109–143.

Baldwin, E. T., Harris, M. S., Yem, A. W., Wolfe, C. L., Vosters, A. F., Curry, K. A., Murray, R. W., Bock, J. H., Marshall, V. P., Cialdella, J. I., Merchant, M. H., Choi, G. & Deibel, M. R. (2002). *J. Biol. Chem.* **277**, 31163–31171.

Boucher, H. W. & Corey, G. R. (2008). *Clin. Infect. Dis.* **46**, Suppl. 5, S344–S349.

Boucher, H. W., Talbot, G. H., Bradley, J. S., Edwards, J. E., Gilbert, D., Rice, L. B., Scheld, M., Spellberg, B. & Bartlett, J. (2009). *Clin. Infect. Dis.* **48**, 1–12.

Bradford, M. M. (1976). *Anal. Biochem.* **72**, 248–254.

Brünger, A. T. (1992). *Nature (London)*, **355**, 472–475.

Cai, J., Han, C., Hu, T., Zhang, J., Wu, D., Wang, F., Liu, Y., Ding, J., Chen, K., Yue, J., Shen, X. & Jiang, H. (2006). *Protein Sci.* **15**, 2071–2081.

Chen, D. Z., Patel, D. V., Hackbarth, C. J., Wang, W., Dreyer, G., Young, D. C., Margolis, P. S., Wu, C., Ni, Z.-J., Trias, J., White, R. J. & Yuan, Z. (2000). *Biochemistry*, **39**, 1256–1262.

Chen, V. B., Arendall, W. B., Headd, J. J., Keedy, D. A., Immormino, R. M., Kapral, G. J., Murray, L. W., Richardson, J. S. & Richardson, D. C. (2010). *Acta Cryst.* D**66**, 12–21.

Clements, J. M., Beckett, R. P., Brown, A., Catlin, G., Lobell, M., Palan, S., Thomas, W., Whittaker, M., Wood, S., Salama, S., Baker, P. J., Rodgers, H. F., Barynin, V., Rice, D. W. & Hunter, M. G. (2001). *Antimicrob. Agents Chemother.* **45**, 563–570.

Credito, K., Lin, G., Ednie, L. M. & Appelbaum, P. C. (2004). *Antimicrob. Agents Chemother.* **48**, 4033–4036.

DeLano, W. L. (2002). *PyMOL*. http://www.pymol.org.

Emsley, P., Lohkamp, B., Scott, W. G. & Cowtan, K. (2010). *Acta Cryst.* D**66**, 486–501.

Fisher, J. F. & Mobashery, S. (2006). *Cancer Metastasis Rev.* **25**, 115–136.

Fritsche, T. R., Sader, H. S., Cleeland, R. & Jones, R. N. (2005). *Antimicrob. Agents Chemother.* **49**, 1468–1476.

Fu, H., Karlsson, J., Bylund, J., Movitz, C., Karlsson, A. & Dahlgren, C. (2006). *J. Leukoc. Biol.* **79**, 247–256.

Gill, S. R. *et al.* (2005). *J. Bacteriol.* **187**, 2426–2438.

Grujic, M., Zavasnik-Bergant, T., Pejler, G. & Renko, M. (2005). *Cancer Lett.* **223**, 211–218.

Guay, D. R. (2007). *Ther. Clin. Risk Manag*, **3**, 513–525.

Guillon, J.-M., Mechulam, Y., Schmitter, J. M., Blanquet, S. & Fayat, G. (1992). *J. Bacteriol.* **174**, 4294–4301.

Guilloteau, J.-P., Mathieu, M., Giglione, C., Blanc, V., Dupuy, A., Chevrier, M., Gil, P., Famechon, A., Meinnel, T. & Mikol, V. (2002). *J. Mol. Biol.* **320**, 951–962.

Hu, Y.-J., Wei, Y., Zhou, Y., Rajagopalan, P. T. R. & Pei, D. (1999). *Biochemistry*, **38**, 643–650.

Klevens, R. M., Edwards, J. R., Tenover, F. C., McDonald, L. C., Horan, T. & Gaynes, R. (2006). *Clin. Infect. Dis.* **42**, 389–391.

Kreusch, A., Spraggon, G., Lee, C. C., Klock, H., McMullan, D., Ng, K., Shin, T., Vincent, J., Warner, I., Ericson, C. & Lesley, S. A. (2003). *J. Mol. Biol.* **330**, 309–321.

Krissinel, E. & Henrick, K. (2007). *J. Mol. Biol.* **372**, 774–797.

Lee, S. K., Choi, K. H., Lee, S. J., Lee, J. S., Park, J. Y., Kim, B. M. & Lee, B. J. (2011). *Bioorg. Med. Chem. Lett.* **21**, 133–136.

Lee, S. K., Choi, K. H., Lee, S. J., Suh, S. W., Kim, B. M. & Lee, B. J. (2010). *Bioorg. Med. Chem. Lett.* **20**, 4317–4319.

Lee, M. D., She, Y., Soskis, M. J., Borella, C. P., Gardner, J. R., Hayes, P. A., Dy, B. M., Heaney, M. L., Philips, M. R., Bornmann, W. G., Sirotnak, F. M. & Scheinberg, D. A. (2004). *J. Clin. Invest.* **114**, 1107–1116.

Leeds, J. A. & Dean, C. R. (2006). *Curr. Opin. Pharmacol.* **6**, 445–452.

Mader, D., Rabiet, M.-J., Boulay, F. & Peschel, A. (2010). *Microbes Infect.* **12**, 415–419.

Margolis, P. S., Hackbarth, C. J., Young, D. C., Wang, W., Chen, D., Yuan, Z., White, R. & Trias, J. (2000). *Antimicrob. Agents Chemother.* **44**, 1825–1831.

Mazel, D., Pochet, S. & Marlière, P. (1994). *EMBO J.* **13**, 914–923.

Meinnel, T., Mechulam, Y. & Blanquet, S. (1993). *Biochimie*, **75**, 1061–1075.

Molteni, V., He, X., Nabakka, J., Yang, K., Kreusch, A., Gordon, P., Bursulaya, B., Warner, I., Shin, T., Biorac, T., Ryder, N. S., Goldberg, R., Doughty, J. & He, Y. (2004). *Bioorg. Med. Chem. Lett.* **14**, 1477–1481.

Moon, J. H., Park, J. K. & Kim, E. E. (2005). *Proteins*, **61**, 217–220.

Moy, F. J., Chanda, P. K., Chen, J., Cosmi, S., Edris, W., Levin, J. I., Rush, T. S., Wilhelm, J. & Powers, R. (2002). *J. Am. Chem. Soc.* **124**, 12658–12659.

Murshudov, G. N., Skubák, P., Lebedev, A. A., Pannu, N. S., Steiner, R. A., Nicholls, R. A., Winn, M. D., Long, F. & Vagin, A. A. (2011). *Acta Cryst.* D**67**, 355–367.

National Committee for Clinical Laboratory Standards (2003). *Susceptibility Testing of Mycobacteria, Nocardia, and Other Aerobic Actinomycetes.* Approved Standard M24-A. Wayne, PA: National Committee for Clinical Laboratory Standards.

Nguyen, K. T., Hu, X., Colton, C., Chakrabarti, R., Zhu, M. X. & Pei, D. (2003). *Biochemistry*, **42**, 9952–9958.

Otwinowski, Z. & Minor, W. (1997). *Methods Enzymol.* **276**, 307–326.

Pichota, A. *et al.* (2008). *Bioorg. Med. Chem. Lett.* **18**, 6568–6572.

Ragusa, S., Mouchet, P., Lazennec, C., Dive, V. & Meinnel, T. (1999). *J. Mol. Biol.* **289**, 1445–1457.

Rajagopalan, P. T. & Pei, D. (1998). *J. Biol. Chem.* **273**, 22305–22310.

Ramanathan-Girish, S., McColm, J., Clements, J. M., Taupin, P., Barrowcliffe, S., Hevizi, J., Safrin, S., Moore, C., Patou, G., Moser, H., Gadd, A., Hoch, U., Jiang, V., Lofland, D. & Johnson, K. W. (2004). *Antimicrob. Agents Chemother.* **48**, 4835–4842.

Robien, M. A., Nguyen, K. T., Kumar, A., Hirsh, I., Turley, S., Pei, D. & Hol, W. G. J. (2004). *Protein Sci.* **13**, 1155–1163.

Rosenthal, V. D. *et al.* (2010). *Am. J. Infect. Control*, **38**, 95–104.

Smith, K. J., Petit, C. M., Aubart, K., Smyth, M., McManus, E., Jones, J., Fosberry, A., Lewis, C., Lonetto, M. & Christensen, S. B. (2003). *Protein Sci.* **12**, 349–360.

Solbiati, J., Chapman-Smith, A., Miller, J. L., Miller, C. G. & Cronan, J. E. (1999). *J. Mol. Biol.* **290**, 607–614.

Spellberg, B., Powers, J. H., Brass, E. P., Miller, L. G. & Edwards, J. E. (2004). *Clin. Infect. Dis.* **38**, 1279–1286.

Vagin, A. & Teplyakov, A. (2010). *Acta Cryst.* D**66**, 22–25.

Watters, A. A., Jones, R. N., Leeds, J. A., Denys, G., Sader, H. S. & Fritsche, T. R. (2006). *J. Antimicrob. Chemother.* **57**, 914–923.

World Health Organization (2004). *World Health Report 2004*, Annex Table 2. http://www.who.int/whr/2004/annex/topic/en/annex_2_en.pdf.

Xu, Y., Lai, L. T., Gabrilove, J. L. & Scheinberg, D. A. (1998). *Clin. Cancer Res.* **4**, 171–176.

Yoon, H.-J., Kim, H. L., Lee, S.-K., Kim, H.-W., Kim, H.-W., Lee, J. Y., Mikami, B. & Suh, S. W. (2004). *Proteins*, **57**, 639–642.

Zhou, Z., Song, X., Li, Y. & Gong, W. (2004). *J. Mol. Biol.* **339**, 207–215.